Caveolar endocytosis of simian virus 40 reveals a new two-step vesicular-transport pathway to the ER

Lucas Pelkmans*, Jürgen Kartenbeck† and Ari Helenius*‡

*Institute of Biochemistry, Swiss Federal Institute of Technology, Universitaetstrasse 16, CH-8092 Zürich, Switzerland
†German Cancer Research Center (DKFZ) Heidelberg, Im Neuenheimer Feld 280, D-69120 Heidelberg, Germany
‡e-mail: ari.helenius@bc.biol.ethz.ch

Simian virus 40 (SV40) is unusual among animal viruses in that it enters cells through caveolae, and the internalized virus accumulates in a smooth endoplasmic reticulum (ER) compartment. Using video-enhanced, dual-colour, live fluorescence microscopy, we show the uptake of individual virus particles in CV-1 cells. After associating with caveolae, SV40 leaves the plasma membrane in small, caveolin-1-containing vesicles. It then enters larger, peripheral organelles with a non-acidic pH. Although rich in caveolin-1, these organelles do not contain markers for endosomes, lysosomes, ER or Golgi, nor do they acquire ligands of clathrin-coated vesicle endocytosis. After several hours in these organelles, SV40 is sorted into tubular, caveolin-free membrane vesicles that move rapidly along microtubules, and is deposited in perinuclear, syntaxin 17-positive, smooth ER organelles. The microtubule-disrupting agent nocodazole inhibits formation and transport of these tubular carriers, and blocks viral infection. Our results demonstrate the existence of a two-step transport pathway from plasma-membrane caveolae, through an intermediate organelle (termed the caveosome), to the ER. This pathway bypasses endosomes and the Golgi complex, and is part of the productive infectious route used by SV40.

Many animal viruses take advantage of receptor-mediated endocytosis to enter their host cells. Typically, they are internalized by clathrin-coated vesicles and penetrate the membrane in endosomes through acid-activated processes[1,2]. The fact that SV40, a non-enveloped DNA virus of the papovavirus family, deviates from this pattern was first discovered by electron microscopy[3–5]. On the cell surface, virions were found to be trapped in small, tight-fitting invaginations that were later found to represent caveolae[6–8]. Virions were then seen in small, non-clathrin-coated vesicles in the cytosol, and after 15-30 min were increasingly present within tubular membrane-bound organelles, each of which contained several virus particles[5]. Starting 4–6 h after uptake, the virus accumulated in an anastomizing, tubular membrane network associated with the ER, where it remained for a long time[5,9]. When a large number of virions was added to cells, these smooth ER networks expanded in size, reaching several μm in diameter[5].

It is now well established that SV40 uses major histocompatibility complex (MHC) class I antigens as its cell-surface receptor, and that the productive infectious pathway involves caveolae. Accordingly, infection is blocked by addition of antibodies against MHC class I antigens[7,10], by administration of cholesterol-depleting drugs that inhibit formation of caveolae[8], and by expression of dominant negative mutants of caveolin-3, a principal protein component of caveolae[11].

The extent to which caveolae participate in constitutive endocytic processes in the cell is still unclear. However, caveolar internalization of gold-conjugated albumin, glycosyl phosphatidyl inositol (GPI)-anchored folate receptor (GM1), ganglioside-bound cholera toxin, and GPI-anchored alkaline phosphatase has been reported[12–15]. From caveolae, gold-conjugated albumin is thought to travel to endosomes[16], cholera toxin through endosomes and the *trans*-Golgi network to the ER[17], and alkaline phosphatase through unidentified vesicular structures back to the plasma membrane[15]. Movement of caveolin-1 from the plasma membrane to intracellular compartments has also been observed after oxidation or depletion of cholesterol[18,19]. The finding that amino-terminal truncation mutants of caveolin-3 localize to intracellular vesicles that are distinct from early endosomes indicates the possible presence of a unique, intermediate organelle in membrane-transport processes that involve caveolae[11].

To analyse caveolar endocytosis in living cells, we investigated SV40 internalization using dual-colour, video-enhanced, live microscopy with Texas Red-labelled virus and green fluorescent protein (GFP)-tagged caveolin-1 and tubulin. Our results show that transport of SV40 from caveolae to the ER involves two distinct phases, and a unique intermediate sorting compartment that is distinct from endosomes, lysosomes and the Golgi complex.

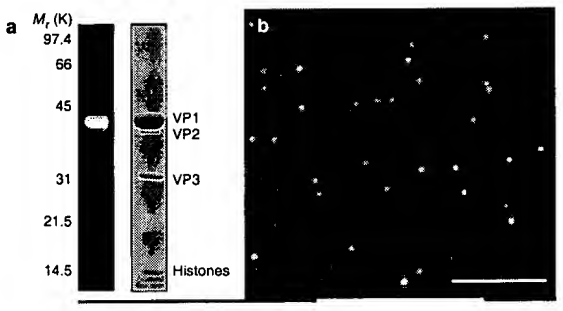

Figure 1 **Texas Red labels the outer capsid proteins of SV40. a**, Analysis of SDS–PAGE-separated, Texas Red-X-labelled SV40 proteins by fluorography (left lane) or Coomassie blue staining (right lane). VP1 (relative molecular mass 41,000) is the only protein that is fluorescently labelled. **b**, Wide-field fluorescence analysis of Texas Red-X-labelled SV40 suspension, showing individual spots of uniform size. Some larger spots probably represent two or three virus particles that are too close to be individually resolved. Scale bar represents 2.7 μm.

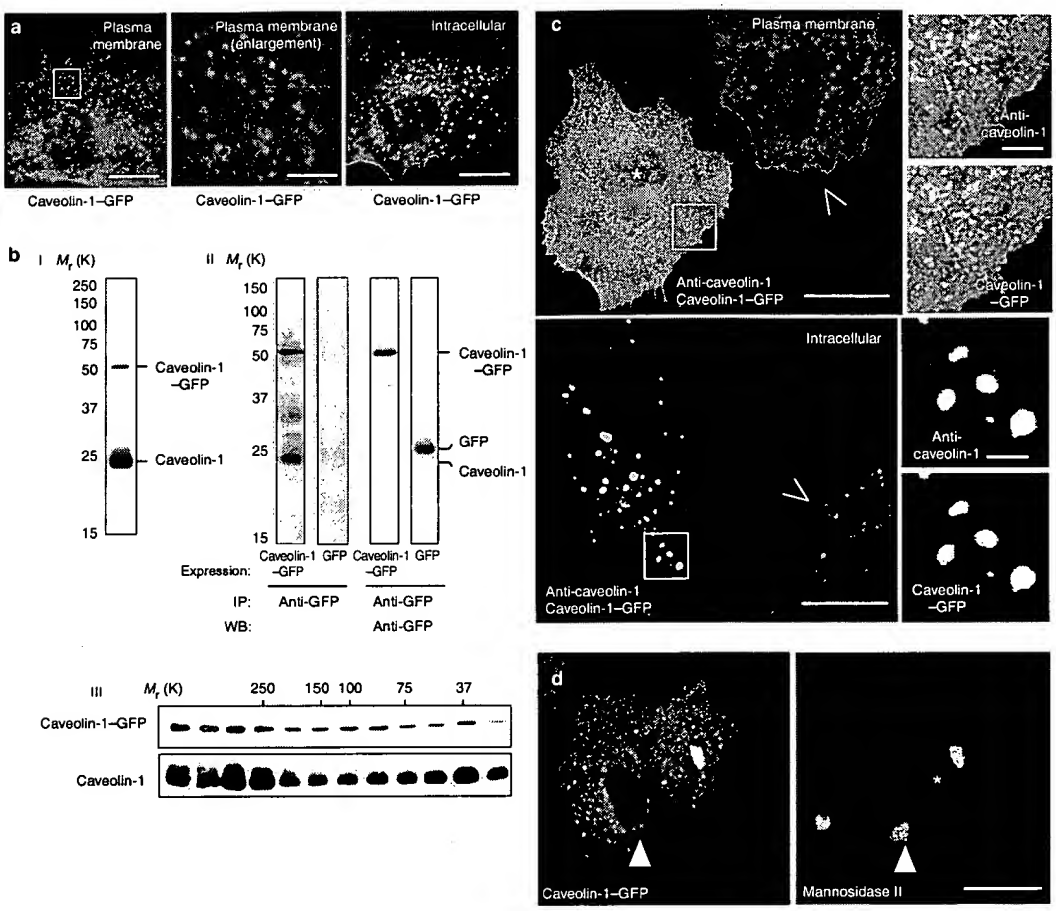

Figure 2 **Caveolin-1–GFP behaves in the same way as endogenous caveolin-1.** **a**, Wide-field fluorescence analysis of CV-1 cells transiently expressing caveolin-1–GFP for 16 h, showing a pattern of spots on the membrane (left and middle panels) that are smaller than spots on fixed cells (compare with **c**) and intracellular vesicles (right panel; see Methods). Scale bars represent 10 μm (left and right panels) and 1 μm (middle panel). **b**, Panel I, western blots of SDS–PAGE-separated lysates of CV-1 cells transiently expressing caveolin-1–GFP for 16 h with an anti-caveolin-1 antibody (N20), showing relative expression levels of caveolin-1–GFP and caveolin-1. Panel II, immunoprecipitation with anti-GFP antibody of lysates of CV-1 cells expressing caveolin-1–GFP, and subsequent western blotting against caveolin-1 (N20; lane 1). In immunoprecipitations of control lysates (GFP; lane 2) no endogenous caveolin-1 was precipitated. Western blotting of these precipitates with anti-GFP antibody (lanes 3, 4) detected only caveolin-1–GFP and GFP. Panel III, high-speed centrifugation of solubilized lysates through a 5–50% sucrose gradient and western blotting against caveolin-1 (N20) shows that a large part of both caveolin-1–GFP and caveolin-1 are present in higher-mass complexes (positions of molecular-mass standards in parallel gradients are shown). **c**, Laser-scanning confocal immunofluorescence analysis of CV-1 cells expressing caveolin-1–GFP (green), using a specific antibody against the caveolar form of caveolin-1 (N20; see Methods). Non-transfected cells show similar patterns (open arrowheads). The occasionally seen Golgi pool of caveolin-1–GFP (asterisk) is not stained by N20. Scale bars represent 7 μm (large panels) and 1 μm (small panels). **d**, Laser-scanning confocal immunofluorescence analysis of caveolin-1–GFP and mannosidase II in CV-1 cells, showing that the occasionally visible perinuclear accumulation of caveolin-1–GFP (asterisk) localizes to the Golgi complex. Caveolin-1–GFP is not present in the Golgi complex (filled arrowheads) in all cells. Scale bar represents 10 μm.

Results

Texas Red-labelled SV40 and caveolin-1–GFP behave normally. To analyse uptake of SV40 in live cells, we labelled purified virus with Texas Red-X (TRX–SV40). After repurification, SDS–polyacrylamide-gel electrophoresis (SDS–PAGE) and fluorography showed that the label was exclusively coupled to the VP1 protein, and absorbance spectra indicated that each virion carried ~10^3 molecules of dye (Fig. 1a). The virus preparation was mono-disperse. Plaque assays showed no loss in infectivity with labelled virus in CV-1 cells, compared with unlabeled virus (3×10^8 plaque-forming units (PFU) per μg of viral protein). Using confocal (data not shown) or wide-field (Fig. 1b) microscopy, the virus suspension was visible as spots of uniform size that probably corresponded to individual virions. The course of early infection was normal, as determined by expression of T-antigen 20 h after addition of virus (see below). As Texas Red staining in cells overlapped exactly with the pattern seen by immunofluorescence using an anti-SV40 polyclonal antibody, we conclude that the dye did not dissociate from the virus during the course of infection (data not shown). This is consistent with our previous observation that degradation of incoming viral proteins is extremely slow[5].

To visualize the distribution of caveolin-1 in live cells, we constructed plasmids encoding enhanced GFP at either the N or the C terminus of canine caveolin-1. When cells were transfected, a similar overall distribution of fluorescent caveolin-1 was observed for both fusion proteins (see below). However, whereas cells expressing

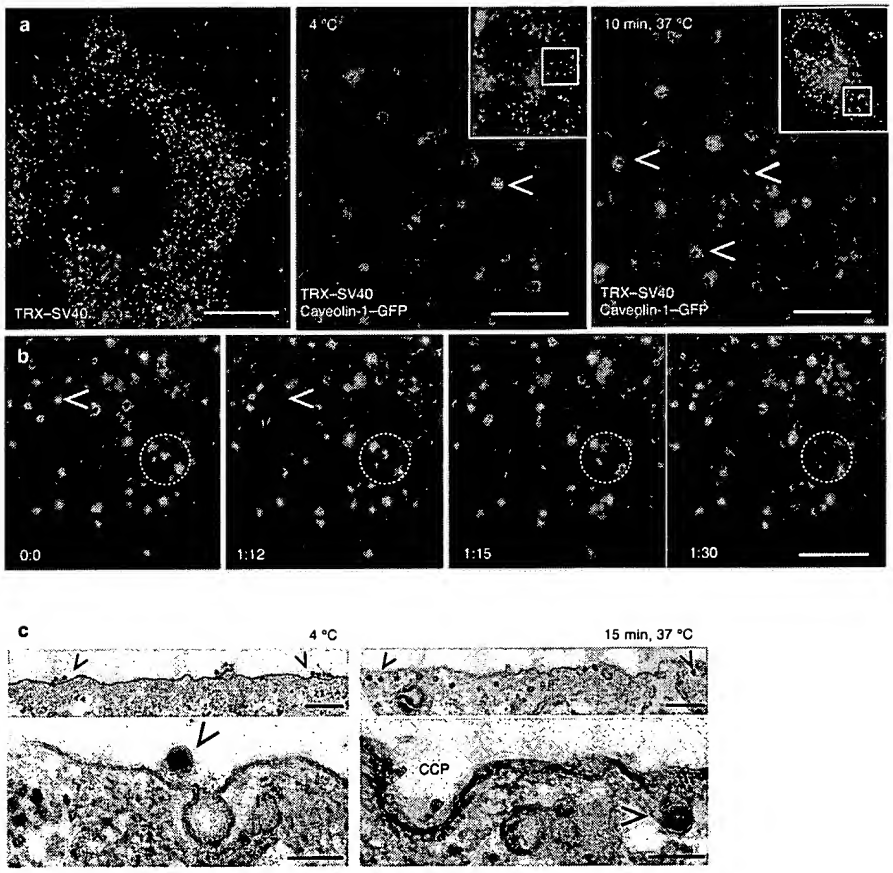

Figure 3 **After binding to the cell surface, SV40 moves into stationary caveolae that are subsequently internalized. a**, Left panel, wide-field fluorescence analysis of plasma-membrane-bound TRX–SV40 on fixed CV-1 cells, showing the spotty pattern of surface-bound virions (*z*-axis position is 0.0 μm; see Methods). Middle panel, fluorescence analysis of fixed CV-1 cells expressing caveolin-1–GFP (green) immediately after binding of TRX–SV40 (red) at 4 °C. TRX–SV40 does not bind directly to caveolin-1–GFP microdomains. One virion is already localized to a caveola (open arrowhead). The image is an enlargement of the square indicated in the inset. Right panel, laser-scanning confocal live fluorescence analysis (pinhole 1.0 a.u.; see Methods) of cells like those described above, rapidly shifted to 37 °C. Within 15 min the majority of TRX–SV40 spots have relocalized to Caveolin-1–GFP microdomains (open arrowheads). The image is an enlargement of the square indicated in the inset. Scale bars represent 10 μm (left panel) and 2 μm (middle and right panels). **b**, Selected frames of a laser-scanning confocal live fluorescence recording (*z*-axis position 0.0 μm, pinhole 1.0 a.u.) at 37 °C of a part of the membrane of caveolin-1–GFP-expressing CV-1 cells bound to TRX–SV40. One spot at the arrowhead and two spots in the circle (upper left of circle) suddenly disappear, whereas others remain in place. Time is shown in min:sec; scale bar represents 2 μm. **c**, Electron micrographs of CV-1 cells fixed either immediately after binding of SV40 for 2 h at 4 °C or after a shift to 37 °C for 15 min. At 4 °C, virions are bound to the membrane (left panels, arrowheads), but are not yet sequestered into caveolae (lower-left panel). After 15 min at 37 °C, most are now sequestered into caveolae (right panels, arrowheads) and not in clathrin-coated pits (CCP). Scale bars represent 500 nm (upper panels) and 100 nm (lower panels).

C-terminally GFP-tagged caveolin-1 allowed normal SV40 infection, N-terminally tagged caveolin served as a dominant negative inhibitor. It prevented uptake of SV40 into cells and inhibited expression of T-antigen (data not shown). This confirmed that the N terminus of caveolin is crucial for caveola-mediated uptake processes[11]. We therefore used C-terminally tagged caveolin-1 (caveolin-1–GFP) for all subsequent experiments.

When viewed in live cells using wide-field microscopy, caveolin-1-GFP staining appeared in two distinct patterns. One pattern consisted of small, scattered spots on the plasma membrane (Fig. 2a, left and middle panels) that probably represent individual caveolae; the other was composed of larger, more brightly stained, intracellular organelles scattered through the cytoplasm (Fig. 2a, right panel). We analysed the amount of caveolin-1–GFP expression in transfected cells by immunoblotting with a polyclonal antibody against the N terminus of caveolin-1 (N20) that recognized both endogenous and GFP-tagged caveolin-1 (Fig. 2b, panel I). Quantification of the bands showed the level of expression of caveolin-1–GFP was ~25% of that of the endogenous protein. As fluorescence microscopy showed that ~50% of cells were transfected, we therefore estimated that the amount of expressed caveolin-1–GFP in cells was ~50% of that of endogenous caveolin-1. High-speed centrifugation of solubilized lysates in sucrose gradients showed that the majority of endogenous and GFP-tagged caveolin-1 was present as oligomers (Fig. 2b, panel III). Furthermore, immunoprecipitation with an anti-GFP antibody brought down both GFP-tagged and endogenous caveolin-1, indicating that they were present as hetero-oligomers (Fig. 2b, panel II).

Indirect immunofluorescence microscopy using the N20 antibody showed that the overall distribution of caveolin-1 was not altered by expression of caveolin-1–GFP (Fig. 2c, open arrowheads). When regions of the plasma membrane were viewed in

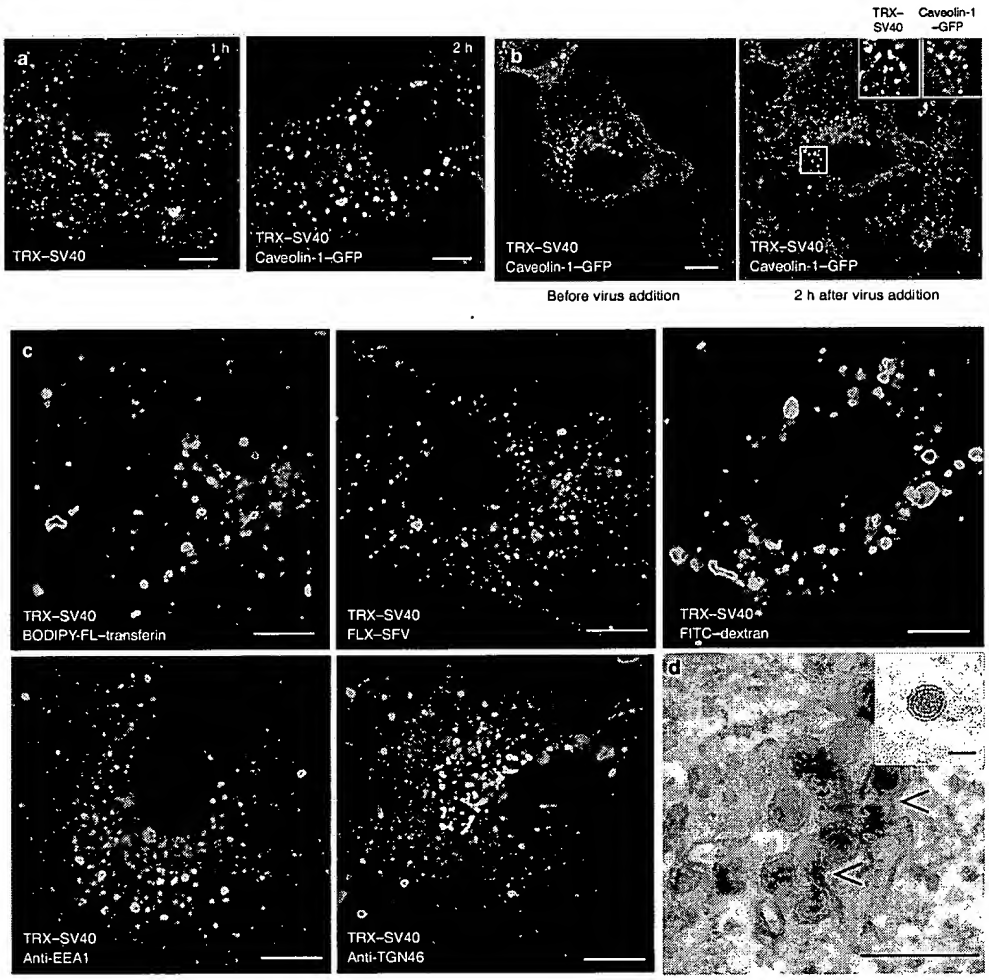

Figure 4 **SV40 enters caveosomes, which are intermediate organelles in caveolar uptake. a**, Left panel, live fluorescence analysis of internalized TRX–SV40 (red) in non-transfected CV-1 cells 1 h after virus binding (z-axis position –0.5 μm; red). Right panel, laser-scanning confocal live microscopy (z-axis position -0.5 μm, pinhole 1.0 a.u.) of CV-1 cells expressing caveolin-1–GFP (green) 2 h after virus binding. **b**, Images obtained at the indicated times from laser-scanning confocal live fluorescence recordings of caveolin-1–GFP-expressing CV-1 cells during addition and subsequent uptake of virus, focusing on intracellular caveolin-1–GFP-containing vesicles (z-axis position –0.5 μm, pinhole 0.2 a.u.). **c**, Upper panels, fluorescence analysis (z-axis position –0.5 μm) of CV-1 cells incubated with BODIPY-FL–transferrin (green), FLX–SFV (green) and FITC–dextran (green) during virus binding and internalization for 1 h at 37 °C, showing that the organelles containing SV40 do not accumulate other endocytic markers. Lower panels, immunofluorescence analysis of a marker of early endosomes (EEA1; green) or the *trans*-Golgi network (TGN46; green) in CV-1 cells at 37 °C 2 h after virus binding, showing that the virus does not accumulate in these organelles. **d**, Thin-section electron micrograph of a typical caveosome 3 h after virus binding and shift to 37 °C, containing multiple virus particles and showing an irregular shape. The membrane lies tightly around virions but is continuous (arrowheads). Inset shows a small vesicle directly after internalization (30 min at 37 °C), which contains only one virion. Scale bars represent 5 μm (**a–c**), 500 nm (**d**) and 50 nm (**d**, inset).

enlargements, it was apparent that the distributions of N20 and caveolin-1–GFP overlapped both at 37 °C (Fig. 2c, left panels) and at 0 °C (data not shown). Complete overlap was also observed in intracellular organelles of most cells (Fig. 2c, enlargements). However, in a small fraction of cells that showed particularly high levels of caveolin-1-GFP expression, we observed an accompanying perinuclear accumulation of caveolin-1–GFP that was not stained by N20 (Fig. 2c, asterisk). Immunofluorescence detection of mannosidase II showed that it this pattern corresponded to the Golgi complex (Fig. 2d). This indicates that caveolin-1–GFP, like endogenous caveolin-1 (ref. 20), has a different conformation when present in caveolae and intracellular spots to that in the Golgi complex. We conclude that caveolin-1–GFP was not greatly overexpressed in cells, that it was a reliable reporter of caveolin-1 distribution, and that it was functional.

After cell-surface binding, SV40 moves to stationary caveolae in the membrane and is internalized. To investigate the initial stages of virus–cell interaction, we allowed TRX–SV40 to bind to CV-1 cells at 4 °C, at which temperature virus internalization does not occur, as determined by electron microscopy[5]. When the cells were fixed, a characteristic spotty pattern of fluorescence was seen on the plasma membrane (Fig. 3a, left panel). Only a few of these TRX–SV40 spots colocalized with caveolin-1–GFP, indicating that the majority of virions did not bind directly to caveolae (Fig. 3a,

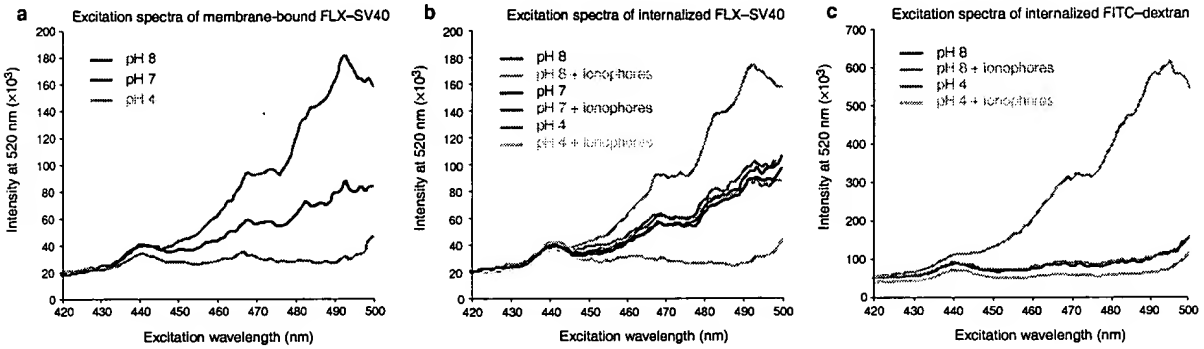

Figure 5 **Caveosomes are not accessible to extracellular proton ions and are at neutral pH. a**, Fluorescence excitation profile of FLX–SV40 bound to the membrane of CV-1 cells for 2 h at 4 °C, showing that spectra are sensitive to extracellular pH (pH 4, 7 or 8). **b**, Similar analysis of FLX–SV40 after internalization for 3 h at 37 °C, showing that spectra are not sensitive to extracellular pH (pH 4, 7 or 8). Addition of 10 μM monensin and nigericin (+ ionophores) resulted in rapid equilibration of spectra to the corresponding extracellular pH. Non-clamped spectra had the same profile as the spectrum clamped at pH 7. **c**, Fluorescence excitation profile of FITC–dextran internalized for 3 h at 37 °C in CV-1 cells, showing the same spectrum at different extracellular pH values (pH 4 and 8). After addition of 10 μM monensin and nigericin the spectra were clamped to the corresponding extracellular pH. Non-clamped spectra have much more acidic profiles than FLX–SV40 (compare with **b**).

middle panel). We confirmed this by electron microscopy (Fig. 3c).

In live cells at 37 °C, TRX–SV40 spots were stationary, except for 10–20% that were laterally mobile (see Supplementary Information, Movie 1). Stationary virions were now associated with caveolin-containing structures. This redistribution occurred so rapidly that by the time a coverslip was moved from ice to a microscope at 37 °C for live fluorescence analysis, most TRX–SV40 had already colocalized with caveolin-1–GFP (Fig. 3a, right panel). Electron microscopy confirmed that after 15 min at 37 °C, the majority of virus particles had localized to caveolae (Fig. 3c).

Although double-positive spots were largely stationary, they could suddenly become mobile and move, within 3–6 s, out of the microscopic plane of focus and into the cell. Using dual-colour live microscopy with a confocal microscope, we observed this movement as the sudden disappearance of spots from the focal plane (Fig. 3b; see Supplementary Information, Movie 2). These results are consistent with a process whereby, after binding to MHC class I antigens, virus particles are mobile in the plane of the membrane until they become trapped in stationary caveolae. Virus-containing caveolae are subsequently internalized, leaving no detectable caveolin-1 behind in the plasma membrane. In a time frame of 3 min, we did not observe internalization of caveolae devoid of virus, indicating that the virus may somehow induce or accelerate the process of caveolar internalization.

Entry into caveosomes — intermediate organelles in caveolar endocytosis. After 0.2–4.0 h of association with cells at 37 °C, the majority of SV40 is known to be intracellular and localized in irregularly-shaped, membrane-bounded organelles[5]. When viewed by wide-field microscopy in live cells incubated with TRX–SV40, these organelles could be seen as brightly fluorescent spots that were dispersed throughout the cytosol and underwent slow, non-directional movements (Fig. 4a, right panel; see Supplementary Information, Movie 3). Most of these spots were positive for caveolin-1–GFP (Fig. 4a, left panel) and resembled, in size and distribution, the caveolin-containing, intracellular organelles that were also seen in the absence of SV40 (Fig. 2a, c). After entry of TRX–SV40 into live cells expressing caveolin-1–GFP, the majority of caveolin-1–GFP-positive organelles that TRX–SV40 entered were indeed already present in the cytoplasm before addition of the virus (Fig. 4b). In other words, most virions were transported to pre-existing caveolin-1-containing organelles.

To investigate whether these organelles are part of the endosomal/lysosomal system, we incubated cells with TRX–SV40 together with two ligands that are known to be internalized by clathrin-mediated endocytosis (BODIPY-FL-labelled transferrin and fluorescein-labelled Semliki Forest virus (FLX–SFV)) or with a fluorescent fluid-phase marker (fluorescein isothiocyanate (FITC)–dextran). After internalization, these had a similar distribution to that of TRX–SV40, although no overlap with TRX–SV40 containing organelles was observed (Fig. 4c). The fact that SV40-containing organelles are distinct from classical endosomes was also indicated by their lack of staining in fixed cells with antibodies against EEA1, a marker protein of early endosomes (Fig. 4c). The distribution of caveolin-1–GFP was distinct from that of EEA1, whether in the presence or absence of SV40 (data not shown). Furthermore, virus-containing organelles did not accumulate Lysotracker green, a lysosomal marker (data not shown), and were not stained by antibodies against TGN46 (Fig. 4c) or mannosidase II (data not shown). These results indicate that these organelles are not related to lysosomes or to the Golgi complex, confirming our previous electron-microscopic observations[5]. Finally, at this intermediate stage of uptake, the distribution of SV40 did not overlap with those of markers of the ER or of the intermediate compartment (data not shown; see below).

Thin-section electron microscopy showed that 2 h after uptake, the majority of virus-containing intracellular organelles were membrane-bound, had irregular shapes and sizes, and contained numerous virus particles (Fig. 4d; see also ref. 5). Although some of these organelles were near the plasma membrane, most were located deeper in the cytoplasm. They clearly differed in size and complexity from the primary endocytic vesicles that contained a single virus particle and which were observed at earlier time points (Fig. 4c, final panel).

To determine whether the virus-containing organelles constitute deep invaginations that are still connected to the plasma membrane, we tested whether extracellular ions could reach the virus after internalization. For this purpose, we labelled SV40 with the fluorophore fluorescein-X (FLX), because its excitation spectrum is pH-sensitive[21]. After binding of FLX–SV40 in the cold, or after internalization at 37 °C for 3 h, we resuspended CV-1 cells in buffers of different pH values (pH 4.0, 7.0 and 8.0) and immediately analysed them with a fluorometer[22]. As expected, the spectrum of membrane-bound FLX–SV40 was sensitive to pH (Fig. 5a). In contrast, the fluorescence emitted by internalized FLX–SV40 did not change (Fig. 5b). After

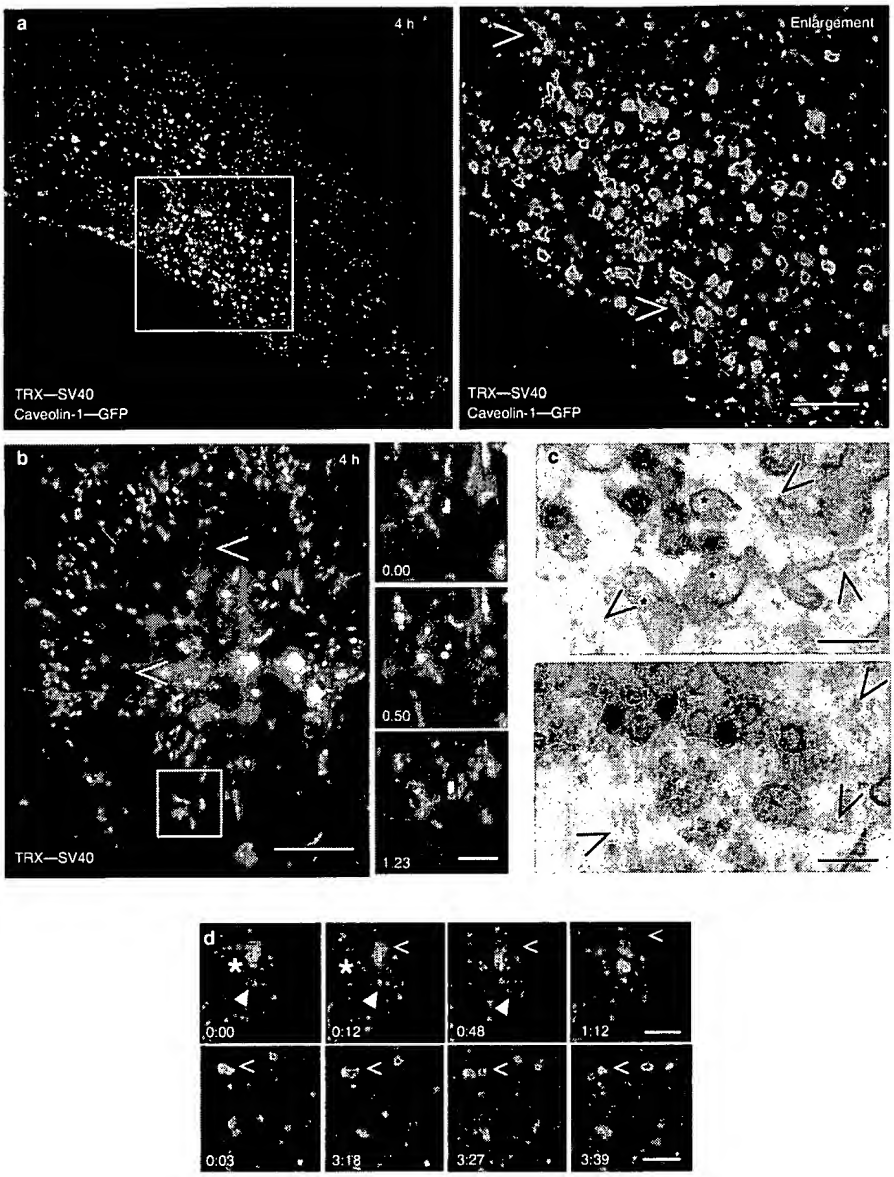

Figure 6 **SV40 is sorted in caveosomes. a**, Laser-scanning confocal live fluorescence analysis (z-axis position –0.5 μm, pinhole 0.2 a.u.) of CV1 cells transfected with caveolin-1–GFP (green) at 37 °C 4 h after virus binding, showing polarization of caveolin-1–GFP and virus in organelles (open arrowheads) that have tubular extensions containing only virus. Enlargement shows the area indicated by the box in the left panel. TRX-SV40 is shown in red. Scale bar represents 10 μm (left panel) or 3 μm (right panel). **b**, Live fluorescence recording (z-axis position –0.5 μm) of a CV-1 cell (left panel), at 37 °C 4 h after virus binding, showing long tubules in the cell (open arrowheads). Small panels show the dynamics of tubule formation in a bigger virus-containing vesicle (times after virus binding are shown in min:sec). Scale bars represent 10 μm (left panel) and 3 μm (right panels). **c**, Thin-section electron micrographs of CV-1 cells at 37 °C 5 h after virus binding, showing tubular extensions containing several virions (upper panel) emerging from vesicular structures (asterisks) that are devoid of virus, and from tubular carriers (lower panel). Microtubules (open arrowheads) were often observed in close proximity. The virus suspension used for these experiments contained both 'full' and 'empty' (lacking DNA) virus particles. Scale bars represent 150 nm. **d**, Selected images, obtained at the indicated times (in min:sec) of part of a CV-1 cell expressing caveolin-1–GFP at 37 °C 4 h after virus binding, showing formation and dissociation of tubular carriers containing only virus from a central caveosome (upper panels, asterisk, filled and open arrowheads) and polarization of a multidomain organelle (lower panels, open arrowheads). Scale bars represent 1 μm.

addition of the ionophores monensin and nigericin[23], the spectrum of internalized FLX–SV40 changed, as the pH of the intracellular organelles was now clamped to the extracellular pH (Fig. 5b). This result clearly demonstrates that the virus-containing compartments were not connected to the plasma membrane.

When we compared the unclamped and pH 7.0-clamped spectra of internalized FLX–SV40 with each other and with that of FITC–dextran (the fluorescence of which is similarly pH-dependent), it was clear that virions were present in a compartment of neutral pH (ref. 24). We conclude that the organelles in which the

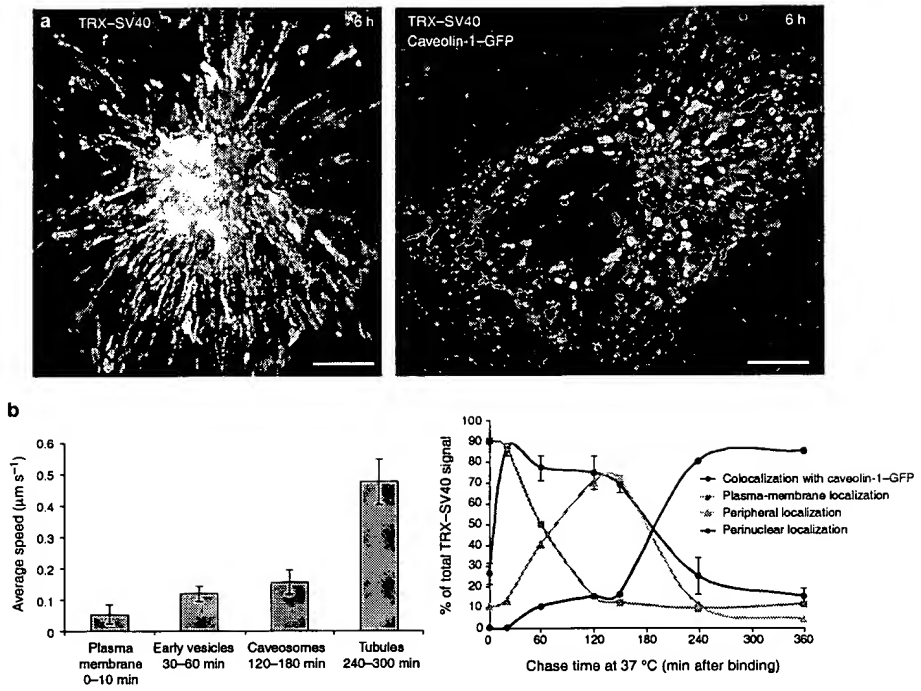

Figure 7 **Entry of SV40 is a two-step process. a**, Live fluorescence analysis (left panel, wide-field microscopy; right panel, dual-colour laser-scanning confocal microscopy; z-axis position –0.5 μm in each case) of cells transfected with caveolin-1–GFP (green) 4 h after virus binding. Images were obtained from merged recordings (50 frames, 500-ms exposure, 2.5-s intervals; see Methods) and show long tracks of fast-moving, perinuclear-orientated carriers (left panel) that only contain virus and originate from caveosomes (right panel, pinhole 0.2 a.u.). TRX-SV40 is shown in red. Scale bars represent 10 μm. **b**, Left panel, quantification of the average speed (see Methods) of moving virus at the plasma membrane 0–10 min after virus binding and shift to 37 °C (9 tracks, 4 cells), 30–60 min after virus binding at 37 °C (early vesicles; 36 tracks, 4 cells) and 120–180 min after virus binding (caveosomes; 42 tracks, 3 cells), and of tubular carriers 240–300 min after virus binding (tubules; 38 tracks, 6 cells). Values are means ± s.e.m. Right panel, quantification of the amount of overlap of TRX–SV40 and caveolin-1–GFP (see Methods) and the amount of TRX–SV40 present in specific regions of interest (see Methods) as a function of time after shift to 37 °C. Values are mean percentages of total virus signal (at least four different cells per time point).

virus was trapped had a pH that was close to neutrality, and that they were not connected with the plasma membrane.

Together, these results show that the majority of incoming SV40 enters a population of pre-existing, caveolin-1-rich, intracellular organelles with a pH of ~7.0; these are distinct from organelles of the classical endocytic and secretory pathways. As they seem to be unique to the caveolar uptake pathway, and as they contain caveolin-1, we have named them 'caveosomes'.

SV40 is sorted from caveosomes. The passage of SV40 within the caveolar endocytic pathway was considerably slower than the transport of ligands within the coated-vesicle-mediated endocytic pathway. Typically, it was ~20 min before the virus was internalized from the plasma membrane and 20–40 min before it reached the caveosomes. A further 2–4 h were needed before the virus started to leave the caveosomes. At this time, video microscopy indicated that caveosomes became more dynamic; their morphology underwent rapid changes and some of them fused with each other. Fission reactions also occurred, and virions could be seen to exit caveosomes in vesicular and tubular structures (see below).

The departure of viruses from caveosomes could be readily visualized by dual-colour, time-lapse microscopic examination of live, caveolin-1–GFP-expressing cells incubated with TRX–SV40 at 37 °C for 4–6 h. From caveosomes, which were yellow in colour, red extensions emerged that were mobile and tubular (Fig. 6a, open arrowheads; see Supplementary Information, Movie 4a–d). These frequently broke off and moved swiftly away from the caveosome. The average length of the tubular structures that detached from caveosomes was ~1 μm, but some were as long as 7 μm (Fig. 6b; see Supplementary Information, Movie 5a–c). As these TRX–SV40-containing tubules were red, they were devoid of detectable caveolin-1–GFP (Fig. 6d, upper panels). Their formation must therefore involve molecular sorting within caveosomes. We were sometimes able to observe separation of red and green signals within a single caveosome, indicating that caveolin-1–GFP and TRX–SV40 were being separated into distinct domains (Fig. 6d; lower panels), each of which could detach from the caveosome as distinct vesicles. Thin-section electron microscopy showed the presence of virus-containing tubular structures, which could be seen attached to vesicular organelles that were devoid of virus (Fig. 6c, upper panel), or as apparently detached structures (Fig. 6c, lower panel). These were often observed in close proximity to microtubules (Fig. 6c, open arrowheads).

Entry of SV40 is a two-step process. The tubular SV40 carriers that emerged from caveosomes were flexible (see Supplementary Information, Movie 5a–c) and moved through the cytosol in the direction of their long axis. Compared with that of slow-moving early vesicles and caveosomes, their movement was rapid, averaging 0.5 μm s^{-1} (Fig. 7a, b). Although individual carriers could be seen to move in both retrograde and anterograde directions, net movement was towards the perinuclear area, which contained the larger organelles in which the fluorescent virus accumulated. A merged picture of all frames obtained over a period of 3–4 min (see Methods) showed that the majority of tracks were positive for TRX–SV40 and negative for caveolin-1–GFP (Fig. 6a, right panel).

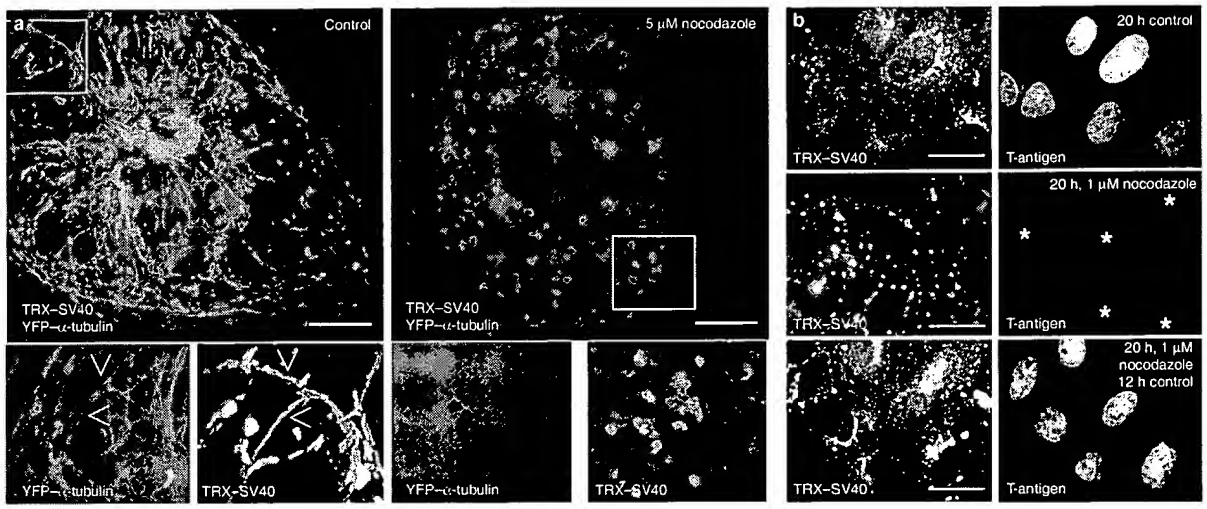

Figure 8 **After sorting, SV40 travels along pre-assembled microtubules to its accumulation site. a**, Live fluorescence analysis (z-axis position –0.5 μm) of stable Ptk2 cells transfected with YFP–α-tubulin (green) at 37 °C 4 h after virus binding, under normal conditions or in the presence of 10 μM nocodazole. Images were obtained as merged recordings (52 frames, 4-s intervals; see Methods). Initial virus entry is not dependent on an intact microtubule skeleton (right panel), but movement towards a perinuclear site is (left panel). Note the long tracks of moving virions in control cells that run along pre-assembled microtubules (small panels on left, open arrowheads); these microtubules are not present in nocodazole-treated cells (small panels on right). TRX–SV40 is shown in red. **b**, Wide-field immunofluorescence analysis (z-axis position –0.5 μm) of T-antigen expression in CV-1 cells at 37 °C 20 h after virus binding, in normal growth medium (upper panels) or in growth medium containing 1 μM nocodazole (middle panels), showing that the majority of TRX–SV40 is in the perinuclear accumulation site when T-antigen is expressed. When transport from caveosomes to the smooth ER is blocked by nocodazole, no accumulation of TRX–SV40 and T-antigen expression is seen (middle panels, asterisks indicate nuclei). After removal of nocodazole and incubation for 12 h in normal medium at 37 °C (lower panels), all TRX–SV40 has now accumulated in the smooth ER and T-antigen expression is observed. Scale bars represent 10 μm.

We next measured the amount of virus in the different cellular locations at different times after entry (Fig. 7b, right panel). We quantified the fluorescent virus signal that was present on the plasma membrane, in caveolae, in caveosomes, and in the perinuclear organelles (see Methods). During the first 20 min, the plasma-membrane-bound virus first associated with caveolae, and were internalized at 37 °C into caveosomes with a half time of 60 min. After 2.5 h, colocalization with caveolin-1–GFP rapidly decreased, and soon thereafter the virus accumulated in perinuclear organelles.

After sorting, SV40-containing carriers travel along microtubules. To investigate the possible function of microtubules in the movement of virions from caveosomes to the perinuclear area, we monitored TRX–SV40-containing carriers in PtK2 cells expressing yellow fluorescent protein (YFP)-tagged α-tubulin. The time course of T-antigen expression, and its sensitivity to cholesterol depletion, indicated that SV40 infects these cells, as is the case in CV-1 cells, through the caveolar pathway (data not shown). Video sequences showed that fast-moving virus carriers were moving along pre-assembled microtubules (Fig. 8a; see Supplementary Information, Movie 6a, b). Although virions appeared to move in both antero- and retrograde directions, the virus eventually accumulated in larger peripheral organelles (see below). Closer analysis showed that the virus-containing tubular structures that budded from caveosomes were already attached to microtubules (see Supplementary Information, Movie 6c, d).

Nocodazole, a drug that disrupts the microtubule cytoskeleton, did not inhibit uptake of virus into CV-1 or PtK2 cells, nor its transport to caveosomes (Fig. 8a). However, virus-containing caveosomes did not enter the dynamic phase, and neither tubular extensions nor tubular carriers were formed. Transport of the virus to perinuclear sites of accumulation was inhibited (Fig. 8a; see Supplementary Information, Movie 7a). Some virus-containing vesicles budded from caveosomes, but did not move away rapidly (see Supplementary Information, Movie 7b). These results show that, although the microtubule network was not needed for transport of SV40 from the plasma membrane to caveosomes, it is evidently essential for efficient transport from caveosomes to the ER.

To investigate whether the microtubule-dependent transport step is needed for productive SV40 infection, we analysed expression of T-antigen 20 h after addition of virus in the presence or absence of nocodazole. In the presence of nocodazole, T-antigen expression was blocked (Fig. 8b, middle panels). No expression of this viral protein was detected even after 48 h (data not shown). When nocodazole was removed after 20 h, the virus accumulated in the smooth ER (see below) and within 12 h T-antigen expression was observed (Fig. 8b, lower panels). We conclude that microtubule-dependent transport of virus to the ER is part of the pathway of productive infection, and that nocodazole blocks infection at a late stage of the entry process.

After sorting, SV40 rapidly accumulates in the smooth ER. After leaving caveosomes, TRX–SV40 accumulated in large, heterogeneous, stationary organelles in the perinuclear region of the cell. The fact that net transport occurred to these organelles was shown by fluorescence recovery after photobleaching (FRAP; Fig. 9a). Four hours after addition of TRX–SV40, we bleached perinuclear regions containing accumulated virus using a high-power laser beam. Upon subsequent incubation at 37 °C, accumulation of new fluorescent virus in the same organelles could be observed by quantitative live fluorescence microscopy (Fig. 9a; see Supplementary Information, Movie 8).

To characterize in more detail the compartment in which incoming SV40 accumulated, we allowed TRX–SV40 to enter CV-1 cells for 16 h. As described above, at this time the virus was present mainly in heterogeneous organelles located in the perinuclear region (Fig. 9b), the largest of which was >8 μm in diameter. These

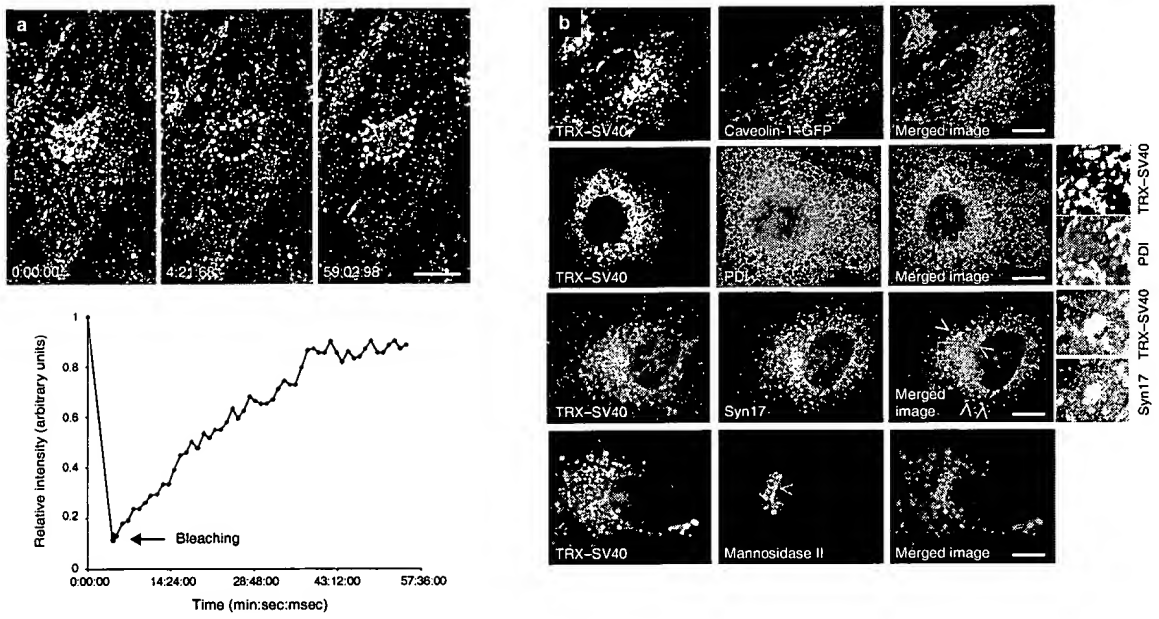

Figure 9 **SV40 finally accumulates in a smooth ER compartment. a**, FRAP analysis (z-axis position–0.5 μm) in CV-1 cells at 37 °C (time is shown in min:s:ms; zero represents 4 h after binding of virus), showing transport to a distinct tubulovesicular organelle (yellow dashed line). Quantification of relative fluorescence intensity (see Methods) of the indicated area, showing that recovery is 90% after ~50 min. **b**, Laser-scanning confocal fluorescence and immunofluorescence analysis (z-axis position–0.5 μm) of the tubulovesicular structures in which SV40 finally accumulates, 16 h at 37 °C after virus binding, showing that they are not positive for caveolin-1–GFP and that the majority is positive for syntaxin 17 (Syn17, arrowheads in enlargements). The compartment is more perinuclear than the reticular ER compartment (PDI) and is partially overlapping, although extensions can be seen that do not overlap with PDI (PDI, red lines in enlargements). SV40 does not accumulate in the Golgi complex (mannosidase II, arrowheads). Scale bars represent 5 μm.

organelles were clearly devoid of caveolin-1–GFP (only 9% overlap; Fig. 9b, uppermost row), and were not stained with antibodies against caveolin-1 (data not shown). When TRX–SV40-loaded cells were analysed by immunofluorescence using antibodies against marker proteins, we found that many (80%) of virus-containing perinuclear organelles were positive for syntaxin17 (Syn17; Fig. 9b, second row), a recently identified marker of smooth ER[25,26]. Some also stained positively for ER markers such as BiP, calnexin (data not shown, see ref. 5) and PDI (70%; Fig. 9b, third row), and for the intermediate-compartment marker ERGIC-53 (54%; data not shown). No significant colocalization with the Golgi marker mannosidase II was observed (5%; Fig. 9b, lowermost row). These organelles did not accumulate Lysotracker green (data not shown), indicating that they are distinct from lysosomes. These results indicate that the tubular network seen in the ER as the site of virus accumulation may correspond to a smooth ER compartment, a conclusion that is consistent with previous electron-microscopic observations[5].

Discussion

Although several ligands and pathogens are known to be internalized through cell-surface caveolae (reviewed in ref. 27), the subsequent intracellular pathways have remained elusive. We have analysed the entry of SV40 into live cells and have visualized their transfer from caveolae in the plasma membrane to the smooth ER. Together with previous observations[5,7,8], our results show that after binding to the cell surface, virions move laterally into caveolae. They apparently trigger a change in the caveolae that results in induction or acceleration of membrane-fission reactions that detach the caveolae from the plasma membrane and allow them to move into the cytoplasm within small, caveolin-1-containing vesicles. Virus particles are delivered by these small vesicles to pre-existing, stationary, membranous organelles that we have called caveosomes. Delivery probably occurs by direct membrane fusion.

Caveosomes are distributed throughout the cytoplasm, are numerous, and are heterogeneous in size and shape. Being considerably larger than the primary, caveolae-derived vesicles, they can contain many SV40 particles. Their membrane contains caveolin-1 in a conformational state that is similar to that in the plasma membrane, but different from that in the Golgi complex. The pH in caveosomes is neutral, and our preliminary experiments with filipin staining indicate that, like caveolae, they are rich in cholesterol (our unpublished observations). The location of caveosomes in the cytosol, their lack of visible connections to the plasma membrane, and their inaccessibility to extracellular protons confirm that they are not connected to the extracellular space.

Two to four hours after arrival of the virus, caveosomes become more dynamic. Although still stationary in the cytoplasm, they begin to undergo rapid shape changes, including formation of long, tubular, virus-containing membrane extensions. After detaching from the caveosomes, these extensions serve as carrier vesicles that transport virions from the caveosomes to the smooth ER compartment in which the virus accumulates. The formation and intracellular movement of these carrier vesicles requires active participation of microtubules. Unlike the primary endocytic vesicles that carry SV40 from the plasma membrane to caveosomes, these carrier vesicles do not contain caveolin-1. At this stage, caveolin-1 is excluded from the virus-containing parts of caveosomes, and seems to cycle back to the plasma membrane in vesicles that are devoid of virus. Although we do not yet know the reason for the gradual change in caveosome dynamics and the activation of its sorting

function, it may be that the caveolar endocytosis pathway is regulated in a complex manner[15].

The fact that the caveolar pathway constitutes the infectious route of SV40 is indicated by the effects of cholesterol-depleting drugs that inhibit both formation of caveolae and virus infection[7,8]. Expression of N-terminally truncated caveolin-3 (ref. 11) and of the N-terminally GFP-tagged caveolin-1 construct described here also inhibit infection. Although other endocytic mechanisms remain active in the presence of these mutant caveolins, SV40 is not internalized from the plasma membrane. We have shown that infection is also blocked by nocodazole, which disrupts the microtubule cytoskeleton and prevents transport of virus from caveosomes to the ER. This indicates that in order to be infectious, the virus must not only be internalized by caveolae but must also be transported to the ER.

Productive infection of SV40 is generally thought to involve penetration of virus particles into the cytosol and subsequent transport through nuclear-pore complexes[28,29]. Using the techniques described here, we have not observed free virus particles in the cytosol or the nucleus, nor have we observed import of fluorescent SV40 VP-1 into the nucleus. Further studies are needed to determine how the genome of the virus moves from the smooth ER to the nucleus.

Although it is clear that caveolae and caveosomes exist in the absence of virus infection, our results do not provide clues as to the physiological function of a caveolae–caveosome–ER pathway. It is possible that it has a role in cholesterol homeostasis — caveolae are rich in cholesterol and raft-forming lipids, and have been implicated in cholesterol regulation[30–35]. As caveolae are also rich in signalling receptors[36], an internalization pathway that bypasses degradative organelles may have other regulatory functions. Recently, it was found that FimH-expressing *Escherichia coli* cells use caveolae to enter phagocytic mast cells[37]. The intracellular compartment in which these bacteria reside and replicate may be related to caveosomes, as it does not fuse with endosomes or lysosomes. Moreover, it is likely that viruses other than SV40 use the caveolar route. Potential candidates include picornaviruses and other non-enveloped viruses that are known to have pH-independent entry mechanisms. Polyomavirus, which is related to SV40, seems to enter a pathway that is similar to that of SV40[4,38,39], although recent observations indicate that caveolin and dynamins may not be involved[40]. □

Methods

Antibodies and reagents.

Polyclonal antisera against mannosidase II, syntaxin 17 and TGN46 are described elsewhere[25,41,42]. Polyclonal antibodies against PDI were from StressGen (Victoria, Canada); monoclonal antibodies against human EEA1 were from Transduction Laboratories; polyclonal antibodies against the N terminus of caveolin-1 (N20) were from Santa Cruz; monoclonal antibodies against GFP were from Boehringer. Polyclonal antiserum against SV40 was raised in rabbits immunized with 200 μg of heat-inactivated SV40 in Freud's adjuvant, according to standard procedures. This serum was able to detect all three structural proteins. FLX–SFV was prepared as described[1], and according to the manufacturer's instructions (Molecular Probes). BODIPY-FL–transferrin, Texas Red-X and fluorescein-X were from Molecular Probes. FITC–dextran (relative molecular mass 42,000) was from Sigma–Aldrich (Steinheim, Germany). Media and reagents for tissue culture were from GibcoBRL. All other chemicals were from Sigma–Aldrich.

Preparation of fluorophore-labelled SV40.

SV40 was purified by a modification of existing protocols[43,44]. Briefly, 24 T175 flasks of confluent CV-1 cells were infected with a stock of SV40 at a multiplicity of infection of 0.01. After 10 days, cells were freeze–thawed three times, and debris was spun down at 10,000*g* for 10 min at 4 °C. The supernatant was saved and the pellet was resuspended in 0.02 volume of supernatant. This suspension was freeze–thawed a further three times and debris was repelleted. Both supernatants were combined and 20 ml were loaded on a 10-ml cushion of HEPES-buffered CsCl (1.4 g ml^{-1}). The virus was banded in the CsCl cushion by centrifugation at 24,000 r.p.m. for 3 h at 4 °C in a SW28 rotor (Beckman). The banded virus was isolated, checked for density (1.34 g ml^{-1}) and diluted five times in fresh HEPES-buffered CsCl (1.34 g ml^{-1}). This suspension was centrifuged to equilibrium at 40,000 r.p.m. for 16 h at 4 °C in a 70.1 Ti rotor (Beckman). The lower virus band was isolated and dialysed extensively against 0.1 M carbonate buffer pH 8.3. The virus was pelleted by centrifugation at 50,000 r.p.m. for 45 min at room temperature in a SW-55 Ti rotor (Beckman), resuspended in 0.1 M carbonate buffer pH 8.3, and stored in aliquots at –80 °C. Virus (1 mg at 1 mg ml^{-1}) was labelled with 33 μl Texas Red-X–succinimidyl ester or fluorescein-X–succinimidyl ester (10 mg ml^{-1} in dimethylsulphoxide) according to the manufacturer's instructions (Molecular Probes). These fluorophores react exclusively with free amines, resulting in a stable carboxamide bond, and contain a seven-atom aminohexanoyl spacer (X), which allows higher degrees of labelling without functional perturbance of the virus. Labelled virus was repurified with CsCl as described above, dialysed against virion buffer (10 mM HEPES pH 7.9, 150 mM NaCl and 1 mM $CaCl_2$) and stored in 2-μg aliquots at –20 °C.

Construction and expression of caveolin-1–GFP.

Caveolin-1–GFP was constructed by polymerase chain reaction (PCR) amplification of canine caveolin-1 complementary DNA from pBluescript-VIP21 (ref. 45), using a standard T3 primer and 5′-CGGTACCGTTGTTTCTTTCTGCATGTTGATGCG, followed by cloning of the *EcoRI–KpnI* fragment from the PCR product into a pEGFP-N1 expression vector (Clontech). The resulting construct contains the canine caveolin-1 gene in frame and upstream of the EGFP sequence with a spacer sequence of 30 nucleotides, 5′-CCGCGGGCCCGGGATCCACC GGTCGCCACC, corresponding to the amino-acid sequence Pro-Arg-Ala-Arg-Asp-Pro-Pro-Val-Ala-Leu. CV-1 cells were grown to 70–90% confluency on 12-mm Alcian Blue-coated coverslips and were transiently transfected with 1.5–3.0 μg of plasmid DNA, using superfect reagent according to the manufacturer's instructions (Qiagen); transfection efficiency was ~50%. Cells, which showed relatively low levels of expression, were analysed after 16–20 h.

Western blotting, sucrose gradients and immunoprecipitation.

CV-1 cells in 6-cm dishes were transiently transfected with caveolin-1–GFP and, after 16 h, lysed in 10 mM Tris–HCl pH 7.5, containing 1% Triton X-100 and protease-inhibitor cocktail. After lysis, nuclei were spun 5,000*g* for 5 min at 4 °C and the postnuclear supernatant was either analysed directly by electrophoresis and immunoblotting or heated for 10 min at 37 °C to dissolve raft domains completely. These lysates were loaded onto a 5–50% linear sucrose gradient containing 10 mM Tris–HCl, pH 7.5, and centrifuged at 4 °C for 18 h at 38,000 r.p.m. in a SW60 rotor (Beckman). Aliquots (500 μ) were collected, TCA-precipitated and analysed for caveolin-1 and caveolin-1–GFP by electrophoresis and immunoblotting. Immunoprecipitation of cell lysates with an anti-GFP antibody was carried out as described[46].

Immunofluorescence microscopy.

Roughly 10^5 CV-1 cells were grown to confluency on 12-mm Alcian blue-coated coverslips and incubated with 1 μg (10^3 PFU per cell) of TRX–SV40 in R-medium (RPMI 1640, 10 mM HEPES pH 6.8 and 0.2% BSA) for 2 h at 4 °C. Cells were washed extensively with ice-cold R-medium and incubated in total growth medium (DMEM, 10% FCS, 1× Glutamax and 1× penicillin/streptomycin) at 5% CO_2 and 37 °C. At the indicated time points, cells were fixed in 4% formaldehyde, quenched with 50 mM NH_4Cl, permeabilized with 0.05% (*w/v*) saponin and then incubated with appropriate primary and secondary antibodies. Coverslips were mounted in Moviol containing DAPCO and examined using a Leica confocal microscope or a Zeiss Axiovert wide-field microscope (see 'Analysis and quantification of images').

Thin-section electron microscopy.

CV-1 cells were fixed, embedded and sectioned as described[3].

pH-dependent excitation scans of FLX-SV40.

CV-1 cells on 6-cm dishes were incubated with 10 μg FLX–SV40 or 5 mg FITC–dextran for 2 h at 4 °C in R-medium. Cells were extensively washed with ice-cold R-medium and either directly resuspended in PBS of different pH values, or further incubated for 3 h in normal growth medium. Cells were transferred to a quartz cuvette with a small stirrer at room temperature and excited with a fluorometer between 420 and 500 nm with 1-nm increments. The light emitted at 520 nm was measured and plotted as light-intensity units. After this, 10 μM monensin and nigericin were added to the same cuvette, incubated for 10 min at room temperature and the same scan was repeated. Data are expressed as averages of four independent experiments, which showed less than 2% variation.

Time-lapse live fluorescence microscopy.

TRX–SV40 was bound to CV-1 cells or to CV-1 cells expressing caveolin-1–GFP and was internalized as described above. Endocytic/lysosomal structures were labelled by binding of TRX–SV40 in the presence of appropriate markers (BODIPY-FL–transferrin, FITC–dextran, FLX–SFV or Lysotracker green) and subsequent internalization as described above. At the indicated times, coverslips were transferred to custom-built aluminium microscope-slide chambers (Workshop Biochemistry, ETH, Zürich) for live analysis in CO_2-independent medium, placed on a heated stage and analysed at 37 °C using wide-field or confocal microscopy. For wide-field microscopy, cells were analysed using a Zeiss Axiovert microscope with a ×100 NA 1.40 plan-apochromat lens. Images were collected using a cooled charge-coupled-device (CCD) camera (Hamamatsu) at 3-s intervals using a computer-controlled shutter with a standard FITC/Texas Red filter set and exposure times of 0.5–1.0 s per image. For confocal microscopy, cells were analysed using an inverted Leica microscope (DM IRBE) with a ×100 NA 1.40 plan-apochromat lens and using computer-controlled excitation with an argon laser at 568 nm (Texas Red) or 488 nm (GFP). Signals were collected at 3-s intervals using a photomultiplier tube (PMT) and were then digitized (1,024 × 1,024 pixels) and converted into images using Leica TCS software. The amount of photobleaching in each channel was analysed by calculating the total fluorescence intensity in each frame of a movie sequence, and was comparable for both signals (Texas Red, 25%; GFP, 20%).

Analysis and quantification of images and video sequences.

For both wide-field and confocal microscopy, CV-1 and PtK2 cells (cell peripheries were extensively spread and had thicknesses of 1.0–1.5 μm) were first focused at the apical plasma membrane; this was set as the reference *z*-axis position of 0.0 μm and was used for plasma-membrane studies. For intracellular analysis of cells, the *z*-axis position was computer-controlled and set at 0.5 μm below the apical membrane (–0.5 μm). In confocal images, the detector pinhole was set at 1 airy-disk unit (a.u.), resulting in a focal-plane thickness of ~120 nm. Where indicated, the pinhole was set at 0.2 a.u. to eliminate out-of-focus signals.

Movies were processed and analysed using the Openlab software package (version 2.0.7; Improvision, Coventry, UK). For single-image presentation of single-colour (TRX–SV40) movie sequences, all images were merged, resulting in tracks that indicate movement. For single-image presentation of dual-colour movie sequences (TRX–SV40 and EGFP–caveolin-1 or TRX–SV40 and YFP–α-tubulin), the TRX–SV40 signal in each image was coloured red, the EGFP–caveolin-1 or YFP–α-tubulin signal in each image coloured green and all images were merged, resulting in tracks that were coloured red, green or yellow, indicating movement of single-positive or double-positive structures. Movements were quantified by marking the position of a specific carrier in at least 20 consecutive images. Average and maximum speeds were calculated by measuring the distance travelled between marked positions in two subsequent images along the whole track. Speed values are expressed as the mean of at least four carriers per movie in at least three different cells.

The amounts of overlap in confocal images were quantified using Adobe Photoshop (version 5.0; Adobe Systems Inc.), by subtracting the green channel from the red channel, resulting in a picture of non-overlapping red elements. Total intensity of the non-overlapping red signal was measured, subtracted from the total red signal, and the resulting overlapping signal is expressed as mean percentage of total red signal (from at least four different cells per time point). Bulk flow of the virus signal was quantified by marking regions of interest in at least four different cells at each time point (all cells were imaged at a z-axis position of –0.5 μm), corresponding to the plasma membrane, the cell periphery and a perinuclear area, as described[47]. However, when prominent accumulation near the nucleus was observed, this whole structure was included in the perinuclear region of interest. Total intensity was measured in regions of interest and was plotted as percentage of total cellular signal.

FRAP data were quantified by measuring the fluorescence intensities of the whole cell and of the bleached area before, directly after and during recovery of bleaching, using the Openlab software. Relative fluorescence intensity of the bleached area over time (R_t) was calculated using the following equation:

$$R_t = \frac{I_{total(0)}}{I_{bleached(0)}} \times \frac{I_{bleached(t)}}{I_{total(t)}} \quad (1)$$

where $I_{total(0)}$ is the total intensity of the cell before bleaching, $I_{bleached(0)}$ is the total intensity of the bleached area before bleaching, $I_{bleached(t)}$ is the intensity of the bleached area over time (directly after bleaching and recovery), and $I_{total(t)}$ is the intensity of the whole cell over time. In this way, data were corrected for overall bleaching during the experiment.

RECEIVED 30 SEPTEMBER 2000; REVISED 4 DECEMBER 2000; ACCEPTED 6 FEBRUARY 2001; PUBLISHED 18 APRIL 2001.

1. Helenius, A., Kartenbeck, J., Simons, K. & Fries, E. On the entry of semliki forest virus into BHK-21 cells. *J. Cell Biol.* **84**, 404–420 (1980).
2. Marsh, M. & Helenius, A. Virus entry into animal cells. *Adv. Virus Res.* **36**, 107–151 (1989).
3. Hummeler, K., Tomassini, N. & Sokol, F. Morphological aspects of the uptake of Simian Virus 40 by permissive cells. *J. Virol.* **6**, 87–93 (1970).
4. Griffith, G. R. & Consigli, R. A. Isolation and characterization of monopinocytotic vesicles containing polyomavirus from the cytoplasm of infected mouse kidney cells. *J. Virol.* **50**, 77–85 (1984).
5. Kartenbeck, J., Stukenbrok, H. & Helenius, A. Endocytosis of simian virus 40 into the endoplasmic reticulum. *J. Cell Biol.* **109**, 2721–2729 (1989).
6. Palade, G. E. Fine structure of blood capillaries. *J. Appl. Physiol.* **24**, 1424 (1953).
7. Stang, E., Kartenbeck, J. & Parton, R. G. Major histocompatibility complex class I molecules mediate association of SV40 with caveolae. *Mol. Biol. Cell* **8**, 47–57 (1997).
8. Anderson, H. A., Chen, Y. & Norkin, L. C. Bound simian virus 40 translocates to caveolin-enriched membrane domains, and its entry is inhibited by drugs that selectively disrupt caveolae. *Mol. Biol. Cell* **7**, 1825–1834 (1996).
9. Maul, G. G., Rovera, G., Vorbrodt, A. & Abramczuk, J. Membrane fusion as a mechanism of Simian Virus 40 entry into different cellular compartments. *J. Virol.* **28**, 936–944 (1978).
10. Breau, W. C., Atwood, W. J. & Norkin, L. C. Class I major histocompatibility proteins are an essential component of the simian virus 40 receptor. *J. Virol.* **66**, 2037–2045 (1992).
11. Roy, S. *et al.* Dominant-negative caveolin inhibits H-Ras function by disrupting cholesterol-rich plasma membrane domains. *Nature Cell Biol.* **1**, 98–105 (1999).
12. Schnitzer, J. E., Oh, P., Pinney, E. & Allard, J. Filipin-sensitive caveolae-mediated transport in endothelium: reduced transcytosis, scavenger endocytosis, and capillary permeability of select macromolecules. *J. Cell Biol.* **127**, 1217–1232 (1994).
13. Montesano, R., Roth, J., Robert, A. & Orci, L. Non-coated membrane invaginations are involved in binding and internalization of cholera and tetanus toxins. *Nature* **296**, 651–653 (1982).
14. Anderson, R. G., Kamen, B. A., Rothberg, K. G. & Lacey, S. W. Potocytosis: sequestration and transport of small molecules by caveolae. *Science* **255**, 410–411 (1992).
15. Parton, R. G., Joggerst, B. & Simons, K. Regulated internalization of caveolae. *J. Cell Biol.* **127**, 1199–1215 (1994).
16. Schnitzer, J. E. & Bravo, J. High affinity binding, endocytosis, and degradation of conformationally modified albumins. Potential role of gp30 and gp18 as novel scavenger receptors. *J. Biol. Chem* **268**, 7562–7570 (1993).
17. Lencer, W. I., Hirst, T. R. & Holmes, R. K. Membrane traffic and the cellular uptake of cholera toxin. *Biochim. Biophys. Acta* **1450**, 177–190 (1999).
18. Smart, E. J., Ying, Y. S., Conrad, P. A. & Anderson, R. G. Caveolin moves from caveolae to the Golgi apparatus in response to cholesterol oxidation. *J. Cell Biol.* **127**, 1185–1197 (1994).
19. Carozzi, A. J., Ikonen, E., Lindsay, M. R. & Parton, R. G. Role of cholesterol in developing T-tubules: analogous mechanisms for T-tubule and caveolae biogenesis. *Traffic* **1**, 326–341 (2000).
20. Dupree, P., Parton, R. G., Raposo, G., Kurzchalia, T. V. & Simons, K. Caveolae and sorting in the trans-Golgi network of epithelial cells. *EMBO J.* **12**, 1597–1605 (1993).
21. Ohkuma, S. & Poole, B. Fluorescence probe measurement of the intralysosomal pH in living cells and the perturbation of pH by various agents. *Proc. Natl Acad. Sci. USA* **75**, 3327–3331 (1978).
22. Maxfield, F. R. in *Acidification of Endocytic Vesicles and Lysosomes.* (eds Pastan, I. & Willingham, M. C.) 235–275 (Plenum, New York, 1985).
23. Maxfield, F. R. Weak bases and ionophores rapidly and reversibly raise the pH of endocytic vesicles in cultured mouse fibroblasts. *J. Cell Biol.* **95**, 676–681 (1982).
24. Mellman, I., Fuchs, R. & Helenius, A. Acidification of endocytic and exocytic pathways. *Annu. Rev. Biochem.* **55**, 663–700 (1985).
25. Steegmaier, M. *et al.* Three novel proteins of the Syntaxin/SNAP-25 family. *J. Biol. Chem.* **273**, 34171–34179 (1998).
26. Steegmaier, M., Oorschot, V., Klumperman, J. & Scheller, R. H. Syntaxin 17 is abundant in steroidogenic cells and implicated in smooth endoplasmic reticulum membrane dynamics. *Mol. Biol. Cell* **11**, 2719–2731 (2000).
27. Anderson, R. G. W. The caveolae membrane system. *Annu. Rev. Biochem.* **67**, 199–225 (1998).
28. Yamada, M. & Kasamatsu, H. Role of nuclear pore complex in simian virus 40 nuclear targeting. *J. Virol.* **67**, 119–130 (1993).
29. Greber, U. & Kasamatsu, H. Nuclear targeting of SV40 and adenovirus. *Trends Cell Biol.* **6**, 189–195 (1996).
30. Fielding, C. J. & Fielding, P. E. Intracellular cholesterol transport. *J. Lipid Res.* **38**, 1503–1521 (1997).
31. Fielding, C. J., Bist, A. & Fielding, P. E. Caveolin mRNA levels are up-regulated by free cholesterol and down-regulated by oxysterols in fibroblast monolayers. *Proc. Natl Acad. Sci. USA* **94**, 3753–3758 (1997).
32. Parton, R. G. Caveolae and caveolins. *Curr. Opin. Cell Biol.* **8**, 542–548 (1996).
33. Simons, K. & Ikonen, E. Functional rafts in cell membranes. *Nature* **387**, 569–572 (1997).
34. Lange, Y., Ye, J., Rigney, M. & Steck, T. L. Regulation of endoplasmic reticulum cholesterol by plasma membrane cholesterol. *J. Lipid Res.* **40**, 2264–2270 (1999).
35. Brown, M. S. & Goldstein, J. L. A proteolytic pathway that controls the cholesterol content of membranes, cells, and blood. *Proc. Natl Acad. Sci. USA* **96**, 11041–11048 (1999).
36. Kurzchalia, T. V. & Parton, R. G. Membrane microdomains and caveolae. *Curr. Opin. Cell Biol.* **11**, 424–431 (1999).
37. Shin, J. S., Gao, Z. & Abraham, S. N. Involvement of cellular caveolae in bacterial entry into mast cells. *Science* **289**, 785–788 (2000).
38. Mackay, R. L. & Consiligi, R. A. Early events in polyoma virus infection: attachment, penetration, and nuclear entry. *J. Virol.* **19**, 620–636 (1976).
39. Griffith, G. R., Marriot, S. J., Rintoul, D. A. & Consilgi, R. A. Early events in polyomavirus infection: fusion of monopinocytotic vesicles with mouse kidney cells. *Virus Res.* **10**, 41–51 (1988).
40. Gilbert, J. M. & Benjamin, T. L. Early steps of polyomavirus entry into cells. *J. Virol.* **74**, 8582–8588 (2000).
41. Velasco, A. *et al.* Cell type-dependent variations in the subcellular distribution of α-mannosidase I and II. *J. Cell Biol.* **122**, 39–51 (1993).
42. Ponnambalam, S. *et al.* Primate homologues of rat TGN38: primary structure, expression and functional implications. *J. Cell Sci.* **109**, 675–685 (1996).
43. Khoury, G. & Lai, C. J. Preparation of simian virus 40 and its DNA. *Methods Enzymol.* **58**, 404–412 (1979).
44. Sahli, R. & Beard, P. in *Cell Biology: A Laboratory Handbook* (ed. Celis, J. E.) 471–478 (Academic, San Diego, 1994).
45. Kurzchalia, T. V. *et al.* VIP21, a 21-kD membrane protein is an integral component of trans-Golgi-network-derived transport vesicles. *J. Cell Biol.* **118**, 1003–1014 (1992).
46. Pelkmans, L. & Helenius, A. Expression of antibody interferes with disulfide bond formation and intracellular transport of antigen in the secretory pathway. *J. Biol. Chem.* **274**, 14495–14499 (1999).
47. Nakano, M. Y. & Greber, U. F. Quantitative microscopy of fluorescent adenovirus entry. *J. Struct. Biol.* **129**, 57–68 (2000).

ACKNOWLEDGEMENTS

We thank all laboratory members for discussions and suggestions throughout this work, M. Kowarik, K. Breiner and M. Molinari for critical reading of the manuscript, and A. Mezzacasa for help with microscopes. We also thank U. Lathinen for cDNA encoding caveolin-1, D. Toomre for Ptk2 cells expressing YFP–α-tubulin, and M. Steegmaier for antibodies against syntaxin 17. This work was supported by the Swiss National Science Foundation and by the Eidgenossische Technische Hochschule Zürich.

Correspondence and requests for materials should be addressed to A.H. Supplementary Information is available on *Nature Cell Biology*'s website (http://cellbio.nature.com).

Movie 1
Dynamics of TRX-SV40 bound to the plasma membrane of CV-1 cells directly after shifting to 37 °C recorded with wide field microscopy. A part of the membrane in which both mobile and stationary spots can be discerned (recorded at 0.33 Hz, shown at 20 Hz, 50 frames). The mobile spots (arrows) move randomly in the membrane. There is considerable bleaching due to the high exposure. Scale bar: 2 μm.

Movie 2
Dynamics of TRX-SV40 and CAV1–GFP on the plasma membrane of CV-1 cells directly after shifting to 37° C recorded with confocal laser scanning microscopy. The movie shows parts of the membrane with TRX-SV40 (red) virions and CAV1-GFP positive microdomains (green), and the resulting yellow spots on the membrane (recorded at 0.33 Hz, shown at 20 Hz, 80 frames). These spots are stationary in the membrane, but that three of them (indicated by arrowheads) disappear, whereas others remain in place. CAV1–GFP is present as a diffusive dynamic staining between the spots. Scale bar: 2 μm.

Movie 3
Dynamics of TRX-SV40 being internalised in CV-1 cells, incubated for 1 h at 37 °C after virus binding before recording with wide field microscopy (recorded at 0.33 Hz, shown at 10 Hz, 50 frames). Small vesicles gain in speed (arrow), by contrast with spots (of about the same size) on the membrane (asterisk), which have not been internalised yet. Some larger vesicles are already visible (arrowhead). The vesicles movements do not share a common orientation. Scale bar: 7 μm.

Movie 4a
Dual-colour live-fluorescence laser scanning confocal microscopy recorded in CAV1–GFP transfected CV-1 cells 4 h after virus binding and shifting to 37 °C (recorded at 0.33 Hz, shown at 10 Hz). The movie shows part of a cell (part of the nucleus is visible in upper left corner) in which virus has accumulated in CAV1–GFP-containing organelles, but is also present in unlabelled vesicles. Arrowheads indicate the formation of multi-domain organelles and separation of virus from a CAV1–GFP containing vesicle. The vesicles are dynamic and they interact frequently in a 'kiss-and-run' fashion. High-speed travelling structures are only positive for virus (red). Scale bar: 2 μm.

Movie 4b
Same as movie 4a, especially focussed on tubule formation from a virus-positive vesicle (lower arrowhead), on which some CAV1–GFP is still located (upper arrowhead). Double positive vesicles (yellow, left upper region) do not move. Scale bar: 2 μm.

Movie 4c
Similar to movie 4a, but at 20 Hz. This enlargement shows the dynamics of sorting indicated by arrowheads. The separation of green and red domains on one organelle (upper arrowhead), and the fast sorting and detachment of virus-positive tubules from double positive vesicles are visible. Scale bar: 5 μm

Move 4d
Similar to movie 4c. Upper arrow, sorting of virus; middle arrow, partial fusion of one double positive vesicle with another (upper arrow) and subsequent fusion. Right arrow, dynamics of several small organelles, as examples of fusion and fission reactions. Scale bar: 5 μm.

Movie 5a
Dynamics of TRX-SV40 targeted to a perinuclear accumulation 6 h after virus binding (recorded at 0.5 Hz, shown at 10 Hz, 50 frames). Large tubular carriers that can span a large part of the cell (arrows) and move both towards and away from the perinuclear accumulation site. In the periphery, dynamics of tubule formation (white box, shown in movie 7a). Scale bar: 5 μm.

Movie 5b
White box in movie 5a, showing the dynamic formation of tubules from a vesicular structure (arrowhead). Note how tubules extend from the vesicular structure and 'search for their way out'. Scale bar: 2 μm.

Movie 5c
The same as movie 5a, from another part of the same cell.

Movie 6a
Dual-colour live-fluorescence microscopy recorded in PtK2 cells expressing YFP-αtubulin, 6 h after virus binding and shifting to 37 °C (recorded at 0.25 Hz, shown at 10 Hz). There is an intricate network of microtubules. Virus has started to accumulate near the nucleus. Tubules containing virus move along pre-assembled microtubule tracks (arrows). Vesicular structures in the periphery are not moving (asterisk, bottom left). There is considerable bleaching of YFP-αtubulin. Scale bar: 10 μm.

Movie 6b
Same as movie 6a, a selection of the upper left region from movie 6a. Scale bar: 10 μm.

Movie 6c and 6d
Same as movie 6a, focussed on vesicular structures from which tubules come out (arrowheads). The tubules grow along the aligning microtubules. Scale bar: 5 μm.

Movie 7a
Same as movie 6, but the cells have been treated with nocodazole throughout the whole experiment. Viruses have entered the cells and have accumulated in vesicular structures, but do not move towards the nucleus. Vesicular structures are dynamic, but show no net movement. There is a large amount of small vesicles. Scale bar: 10 μm.

Movie 7b
Selection of movie 7a (see white box) indicating that fission of bigger vesicular structures results in the formation of multiple small vesicles (arrow), instead of larger tubules. Scale bar: 2 μm.

Movie 8
Fluorescence recovery after photobleaching (FRAP) experiment in CV-1 cells recorded with laser scanning confocal microscopy (recorded at 0.017 Hz, shown at 10 Hz) 6 h after virus binding and shifting to 37 °C. The movie shows a cell which has accumulated a large amount of virus at the perinuclear site, but yet contains a lager amount of carriers. In the second frame, the prominent accumulation (indicated by yellow line) completely disappeared (owing to bleaching with a high power laser beam), and subsequently recovers with newly targeted virus. The structure before and after bleaching is similar. Scale bar: 5 μm.